

Short Communication

Preparation and Phosphating of Yttrium-Based Chemical Conversion Coatings on AZ91D Magnesium Alloy for Corrosion Protection

Baojun Han^{1,2,*}, Dongdong Gu², Yang Yang², Ling Fang^{1,2}, Guanghuai Peng^{1,2}, Chubin Yang^{1,2}

¹ Jiangxi Provincial Engineering Research Center for Magnesium alloys, GanNan Normal University, Ganzhou 341000, PR China

² School of Chemistry and Chemical Engineering, GanNan Normal University, Ganzhou 341000, PR China

*Email: baojunhan@126.com

Received: 2 September 2016 / Accepted: 23 October 2016 / Published: 10 November 2016

The yttrium-based chemical conversion coatings were prepared on AZ91D magnesium alloy by immersing in yttrium nitrate solution firstly, and then in ammonium dihydrogen phosphate ($\text{NH}_4\text{H}_2\text{PO}_4$) solution. The micro-morphology and the composition of the coating were investigated using scanning electron microscopy (SEM), energy dispersive spectroscopy (EDS), X-ray diffraction (XRD) and X-ray photoelectron spectroscopy (XPS), respectively. The results show that the number and size of the cracks in the coating were obviously reduced after phosphating, and the compactness of the yttrium conversion coatings were increased. The phosphated coating was mainly composed of Y_2O_3 , $\text{YO}_{x/y}$, $\text{Mg}_3(\text{PO}_4)_2$, AlPO_4 and YPO_4 . Furthermore, the corrosion resistance of the coating was measured by means of potentiodynamic polarization curves and electrochemical impedance spectroscopy (EIS). Following phosphating, the corrosion potential of the coating was shifted positively about 180mV compared to the uncoated one, and the corrosion current density decreased about one order of magnitude.

Keywords: AZ91D magnesium alloy; yttrium-based conversion coating; phosphating; corrosion resistance

1. INTRODUCTION

Magnesium and its alloys are the lightest structural metallic materials which have many excellent properties, such as low density, good casting ability, favorable bio-compatibility, etc. [1,2]. These properties make Mg alloys as the promising candidates in many fields including aeronautics,

automotive industries, military and consumer electronic industries. However, poor corrosion resistance of magnesium and its alloys seriously limits their applications [3,4]. Among various surface modification techniques [5-11], chemical conversion coating technique has received significant attention during the past years due to its advantages such as uniform deposition, good adhesion and economical [12]. The conventionally used conversion coatings are usually based on chromium compounds that have been proven to be highly toxic carcinogens [13]. Therefore, the development of chromate-free chemical conversion is necessary, and phosphate/permanganate, vanadate, titanate, rare-earth salt and stannate have been proposed as its replacement [14-17]. Among them, rare earth based conversion coatings are considered to be the best candidate for replacing the hexavalent chromium compounds [18]. Rare earth elements, La and Ce were widely adopted to improve the corrosion-resistance capability of magnesium, aluminum and zinc alloys. However, there are few works on the application of yttrium protecting magnesium alloys as large amount of micro-cracks appear in the coating which accelerate the corrosion of the substrate of magnesium alloy [19,20]. It is said, filling and sealing of the connected holes or pores, and cracking can improve barrier effects of the coatings against aggressive medium and the corrosion resistance of substrate. Chemical densification [21] is considered as one of the simplest methods for filling and sealing chemical conversion coating to further improve its corrosion consistence.

In this paper, a novel and environment-friendly chemical densification e.g., phosphating was developed for the yttrium-based chemical conversion coatings on AZ91D magnesium alloy to improve its corrosion resistance. In addition, the microstructure, chemical composition and the corrosion-resistance capability of the composite conversion coatings were investigated.

2. EXPERIMENTAL

2.1 Sample preparation

The substrate material used in this study was commercial AZ91D magnesium alloy with a chemical composition of Mg-9.2Al-0.5Zn (wt. %). The samples were first polished with SiC paper up to 2500 grits, degreased in absolute ethanol in an ultrasonic bath for 900 s, then dipped into a HNO₃ (0.8%) aqueous solution for 15 s and a HF (40%) aqueous solution for 30 s. Between each step of the operation, the samples were rinsed by distilled water in ultrasonic bath to remove all the residues on the surface of the alloy, and dried in a stream of air.

The yttrium-based conversion coating was prepared by immersing the AZ91D magnesium alloy sample in the solution containing 10 g/L yttrium nitrate at 30 °C for 50 min. Then the yttrium conversion coating was phosphated under the parameters shown in Table 1.

Table 1. Phosphating parameters of yttrium-based chemical conversion coatings on AZ91D magnesium alloy

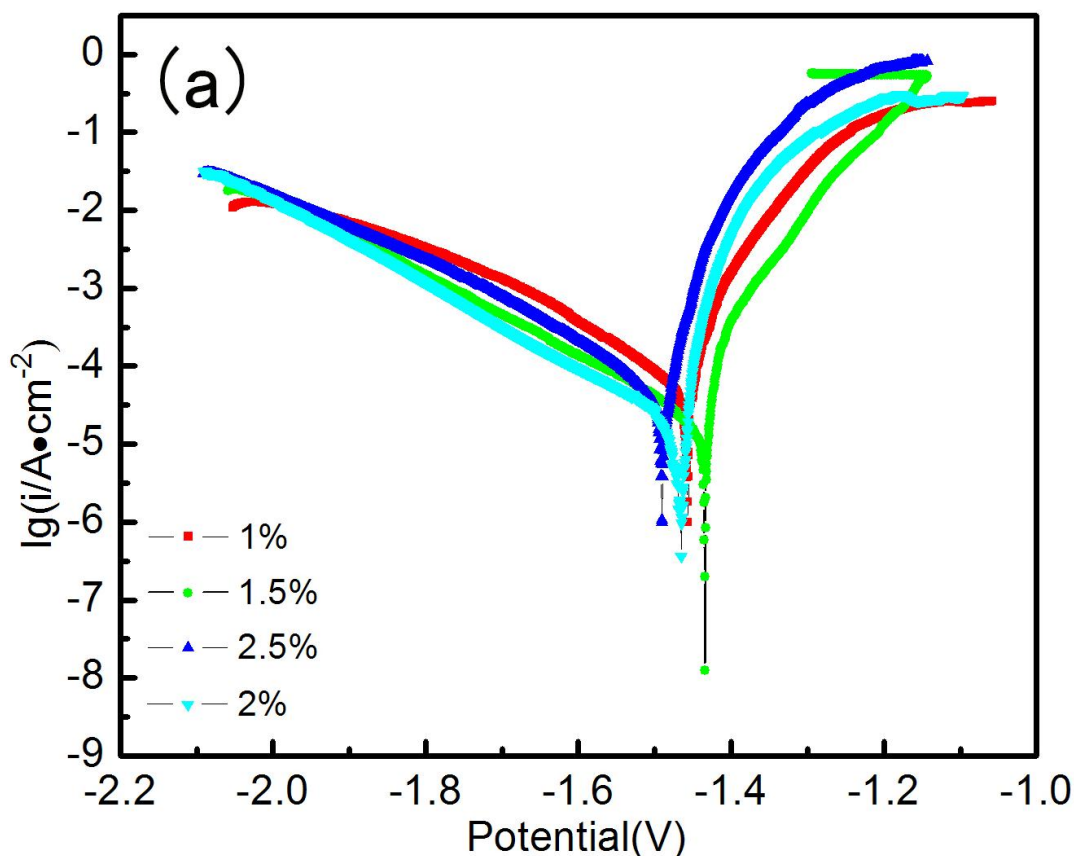
mass fraction of NH ₄ H ₂ PO ₄	Time/s	Temperature/°C
1%-2.5%	30s-180s	75-90

2.2 Characterization

The micro-morphology and the chemical composition of the coatings were examined using a scanning electron microscopy (SEM, Quanta, FEI-450) equipped with Oxford X-ray energy dispersive spectrum (EDS). The phase compositions were characterized using X-ray diffraction (XRD, Bruker D8) with Cu K α radiation over an angle range of 10~90° (2 θ values). The chemical composition of the coating was detected using an X-ray photoelectron spectroscopy (XPS, Physical Electronics, Thermo ESCALAB 250Xi) with Al K α (h ν =1486.6eV) monochromatic source. All spectra were corrected using the signal of C 1s at 284.8 eV. The electrochemical test was conducted using a CHI660B electrochemical workstation (CH Instruments) in a three-electrode cell composed of a reference electrode (a saturated calomel electrode), a counter electrode (a platinum foil) and a working electrode. The area of the working electrode was 1.0 cm². EIS measurements were carried out at a certain corrosion potential in a frequency range from 10⁻² Hz to 10⁵ Hz using a 10 mV amplitude perturbation. The potentiodynamic polarization curves were performed at a scanning rate of 1 mV/s. The corrosion environment was simulated by 3.5% NaCl solution at room temperature.

3. RESULTS AND DISCUSSIONS

3.1 Technical parameters optimization of phosphating



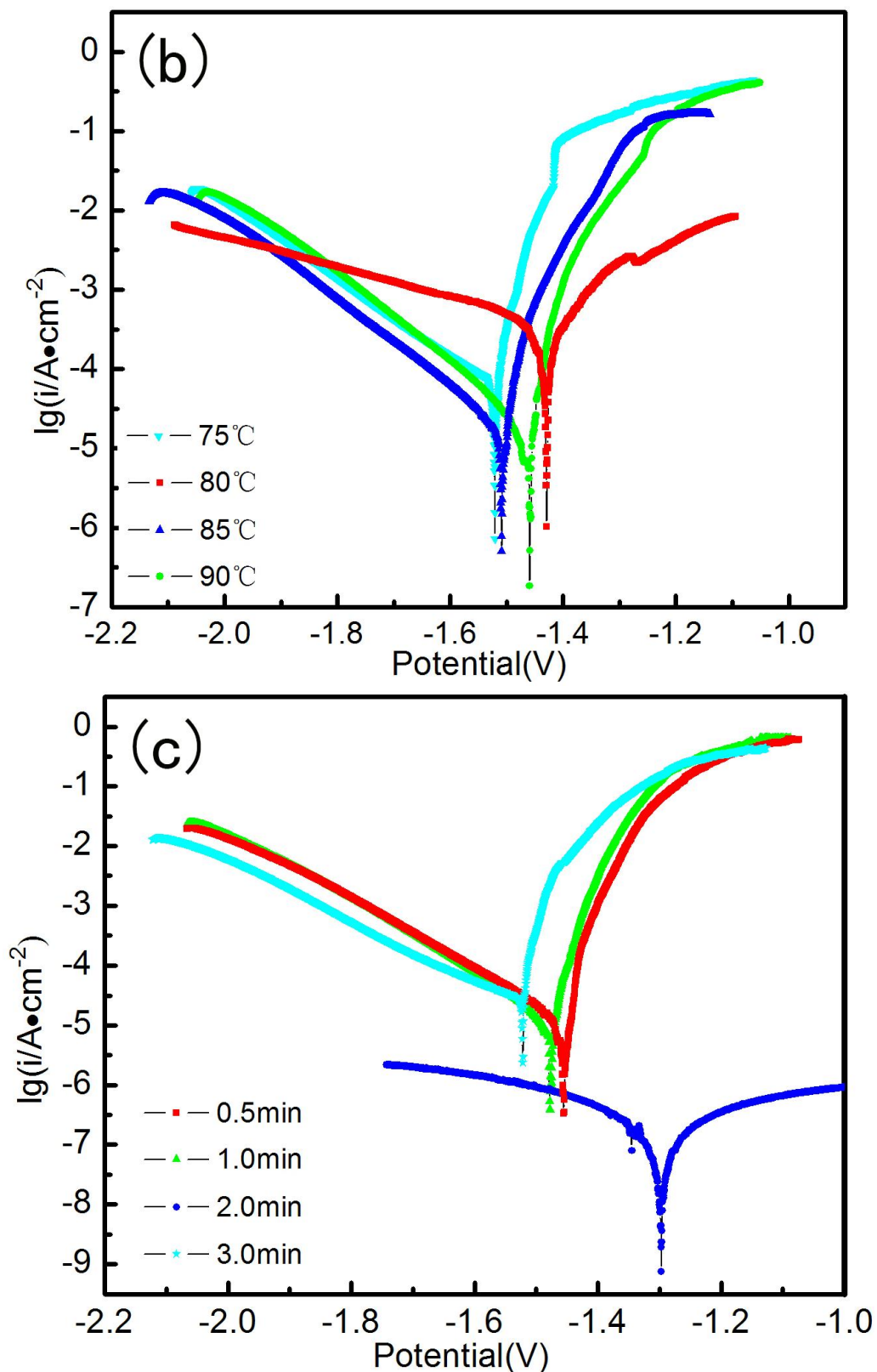


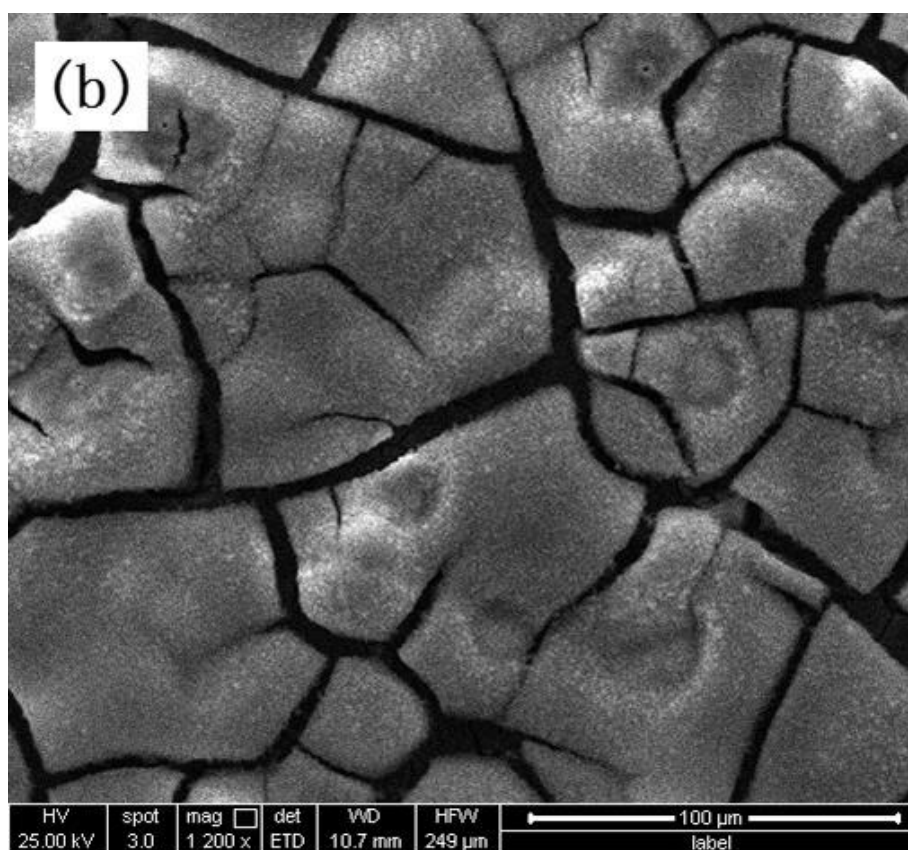
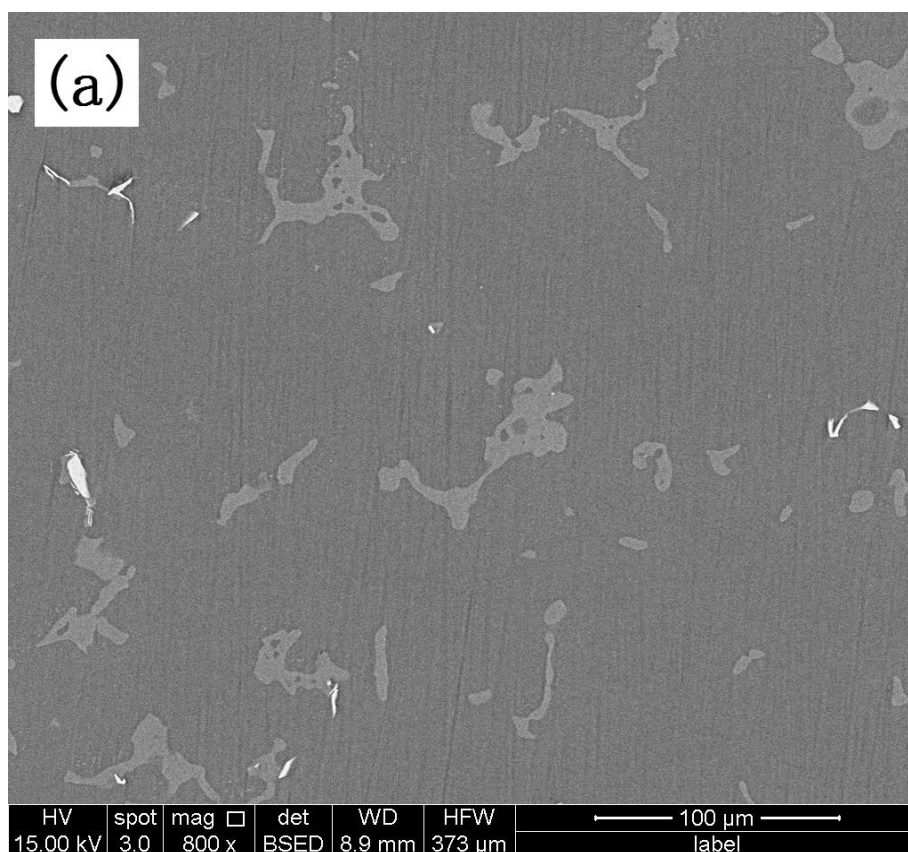
Figure 1. Potentiodynamic curves of yttrium-based coatings on AZ91D magnesium alloy phosphated with (a) 1.0%, 1.5%, 2.0% and 2.5% mass fraction of $\text{NH}_4\text{H}_2\text{PO}_4$, (b) temperature of 75 °C, 80°C ,85°C and 90°C and (c) phosphating time of 0.5 min, 1.0 min, 1.5 min and 2.0 min

Table 2 Experimental conditions and Tafel fitting results of potentiodynamic curves shown in Figure 1

Experimental number	Temperature /°C	Time/ min	mass fraction of NH ₄ H ₂ PO ₄	E _{corr} (mV)	I _{corr} /area (μA/cm ²)	b _c (mV/dec)
1	80	1	1.0%	-1456	49.3	200.5
2	80	1	1.5%	-1433	18.7	171.6
3	80	1	2.0%	-1465	19.6	175.3
4	80	1	2.5%	-1490	53.5	209.1
5	80	0.5	1.5%	-1455	13.3	222.0
6	80	1	1.5%	-1477	12.9	174.6
7	80	2	1.5%	-1297	0.203	155.7
8	80	3	1.5%	-1521	21.7	264.7
9	75	2	1.5%	-1520	54.4	205.4
10	80	2	1.5%	-1450	20.2	175.6
11	85	2	1.5%	1509	21.7	182.7
12	90	2	1.5%	-1511	448.0	549.3

Figure 1 shows the potentiodynamic polarization curves of the yttrium conversion coating prepared with different conditions. As shown in Table 1, the mass fraction of NH₄H₂PO₄, treatment time and treatment temperature are optimized for phosphating process and each factor contained four levels. Table 1 also shows the Tafel fitting parameters of polarization curves shown in Fig.1. It is obvious that the treating time is the most important factor, which means that the treating time has the strongest impact on the corrosion resistance of the coatings. Corrosion current, corrosion potential and cathodic Tafel slopes (b_c) are the main evaluation standards of the corrosion resistance performance of the coating [22-24], and the optimistic treating condition is set as 1.5% mass fraction of NH₄H₂PO₄, 120s and 80 °C. based on the corrosion current, corrosion potential and Tafel slopes (b_c) data analysis of Table 1.

3.2 Morphology and composition of conversion coating



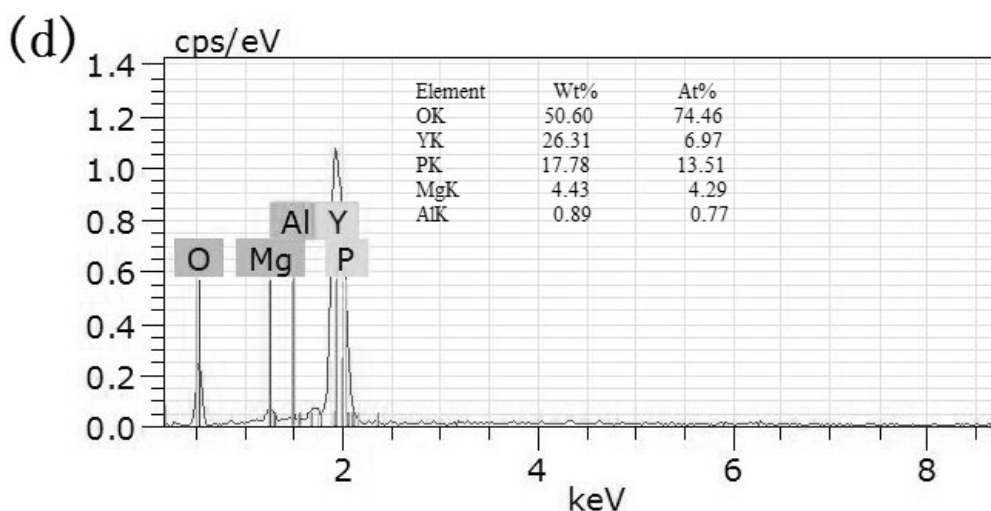
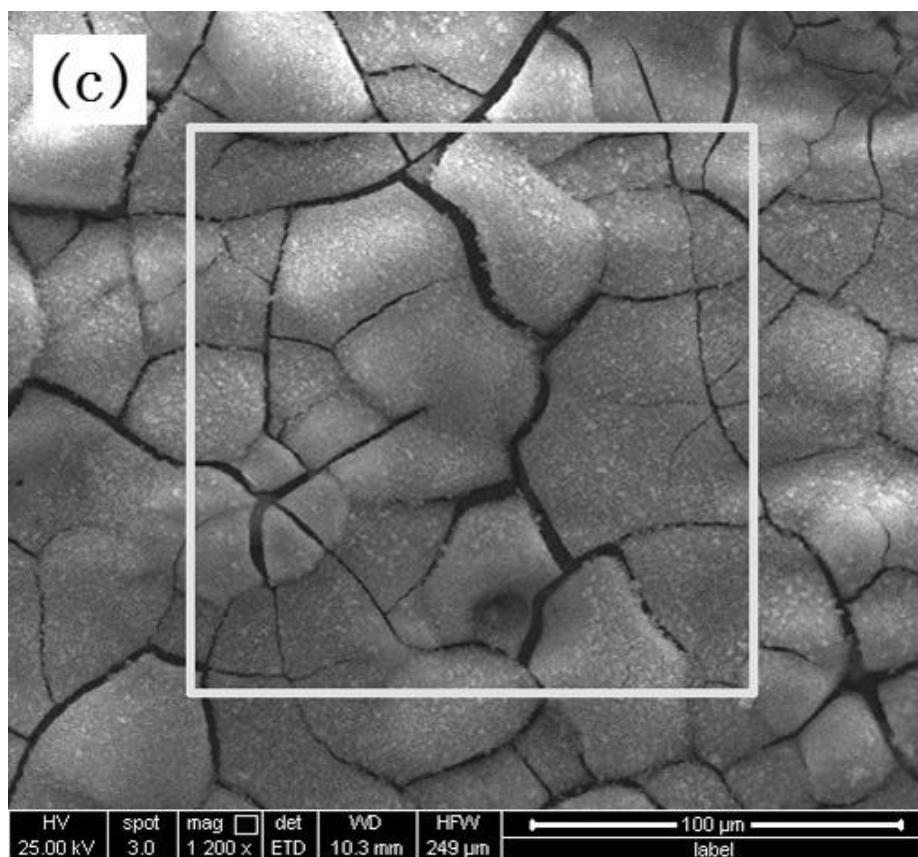
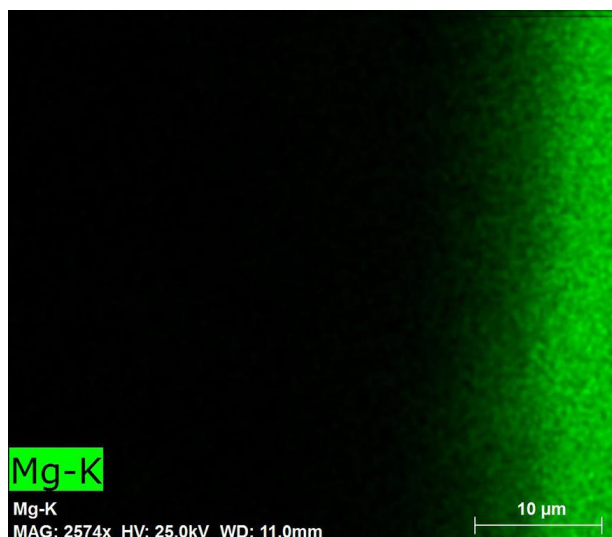
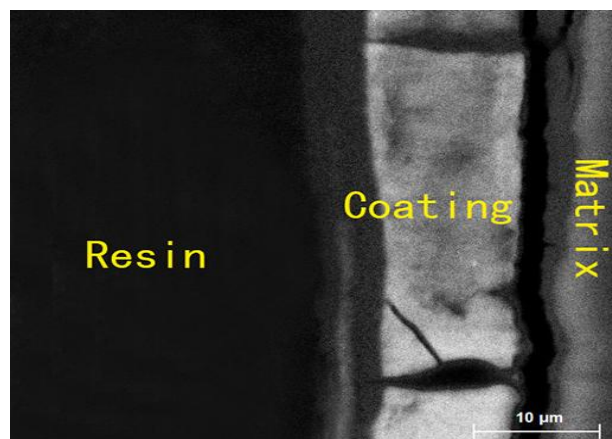


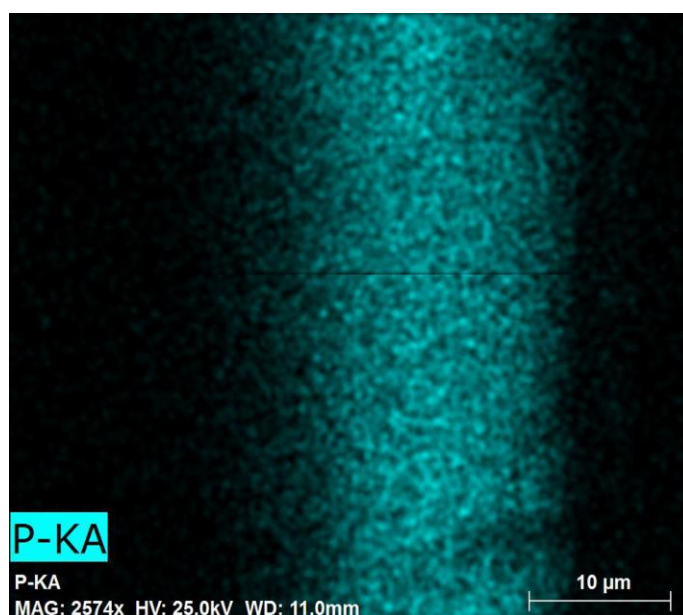
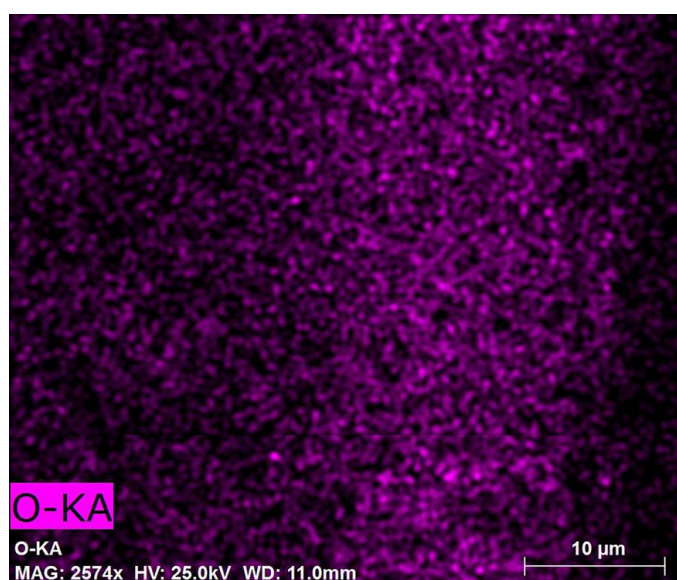
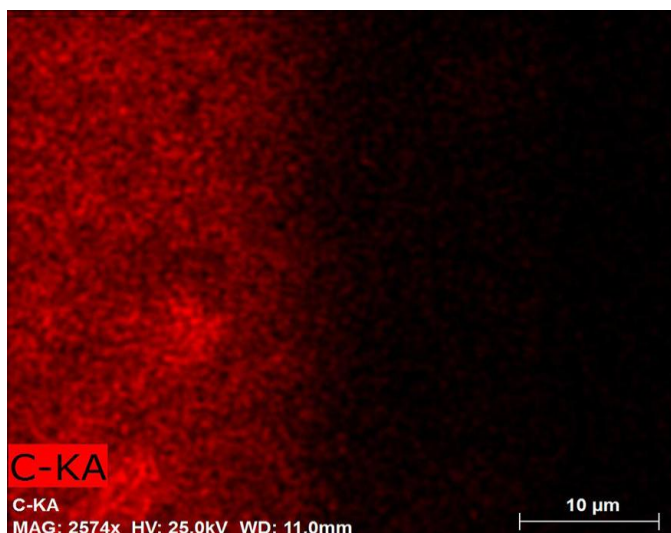
Figure 2. Surface SEM Morphology of AZ91D magnesium alloy (a) uncoated, (b) immersed in solution containing 10 g/L yttrium nitrate at 30 °C for 50 min, (c) immersed in solution containing 10 g/L yttrium nitrate at 30 °C for 50 min and then in solution containing 1.5% mass fraction of $\text{NH}_4\text{H}_2\text{PO}_4$ at 80 °C for 120s and (d) EDS result of the phosphated coating

Fig. 2 shows the surface morphology of the uncoated AZ91D magnesium alloy, the yttrium-based conversion coating and the phosphated conversion coating. Fig. 2a indicates that the uncoated AZ91D magnesium alloy consists of primary α -Mg and irregular discontinuous intermetallic β - $\text{Mg}_{17}\text{Al}_{12}$ phase. Some thick cracks are distributed in the yttrium-based conversion coating (Fig. 2b). It

is reported that hydrogen evolution and higher inner stress result in the formation of cracks [25]. Fig. 2c shows that the cracks in Fig. 2b obviously decrease and the coating becomes compact after phosphating. EDS was employed to determine the compositions of the phosphated sample after chemical densification process. Fig. 2d shows the EDS spectra of the coating which is taken from the rectangular box in Fig. 2c. The EDS results show that the coating is composed of Mg, Y, Al, P and O elements. Among these elements, Al and Mg come from the matrix, Y from the conversion solution, O mainly from the solution and phosphating process, and P from phosphating solution. The above results mean that the phosphating can narrow the cracks on the surface of the yttrium-based conversion coating, which has better uniformity than the yttrium conversion coatings.

Fig. 3 shows the morphology and elemental maps of the phosphate conversion coating. It can be found that the coating thickness was about 10 μm . The compact coating with few thin cracks is observed. As shown in elemental maps, Mg is concentrated in the matrix whereas small amount of Mg can be found near the coating. C mainly distributes in the resin, whereas the element O distributes in matrix, coating and resin, especially in coating. P and Y are enriched in coating, which clearly indicates that the phosphated coating forms on the surface of AZ91D magnesium alloy. Al is also concentrated in matrix and a fraction of Al exists in the coating. All the results indicate that coating is mainly composed of metallic oxide and phosphate oxide.





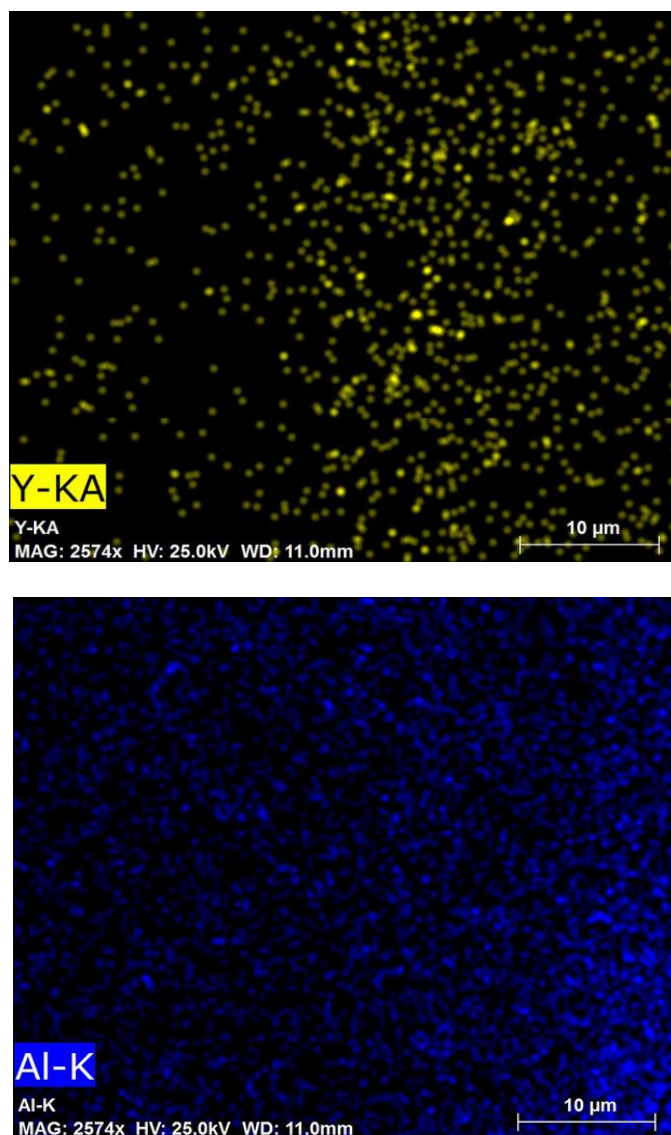


Figure 3. SEM cross-sectional morphology and EDS elemental maps of the yttrium-based conversion coating phosphated in solution containing 1.5% mass fraction of $\text{NH}_4\text{H}_2\text{PO}_4$ at 80 °C for 120s

3.2 XRD and XPS analysis of coating

The XRD patterns of the uncoated and coated AZ91D magnesium alloys are shown in Fig. 4. It indicates that Y_2O_3 peaks are present in Fig. 4 (b) and (c), and furthermore phosphides peaks appear at phosphated sample. Fig. 4c indicates that the composite coating mainly consists of $\text{Mg}_{17}\text{Al}_{12}$, $\text{Mg}_3(\text{PO}_4)_2$, Y_2O_3 and YPO_4 .

XPS was used to identify the specific electron binding energies of the coating and the main reaction products. Fig. 5 shows the XPS spectra of the phosphated yttrium-based coating. It can be found that in addition to Y, Mg, Al, P and O, significant amounts of C is present in the coating, which is common in XPS surface scanning as hydrocarbons comes from the environment. The spectra in Fig. 5b shows the Y 3d3/2 and Y 3d5/2 ionization. The Y 3d3/2 and Y 3d5/2 peaks are measured at 158.2eV and 160.3eV which can be attributed to Y^{3+} coincidence with reference value [26]. This

represents that the conversion coating consists of $YO_{x/y}$ and Y_2O_3 . Fig. 5c shows the high resolution spectrum of P 2p spectra. The P 2p peak is detected at 133.4eV, which can be assigned as PO_4^{3-} according to reference [27] and [28].

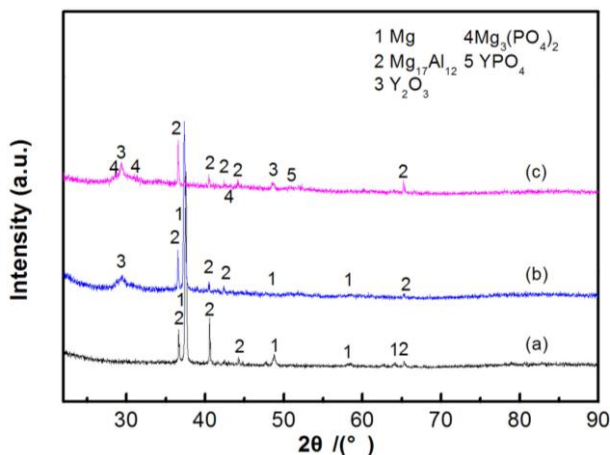


Figure 4. XRD patterns of AZ91D magnesium alloy (a) uncoated, (b) immersed in solution containing 10 g/L yttrium nitrate at 30 °C for 50 min and (c) immersed in solution containing 10 g/L yttrium nitrate at 30 °C for 50 min and then in solution containing 1.5% mass fraction of $NH_4H_2PO_4$ at 80 °C for 120s

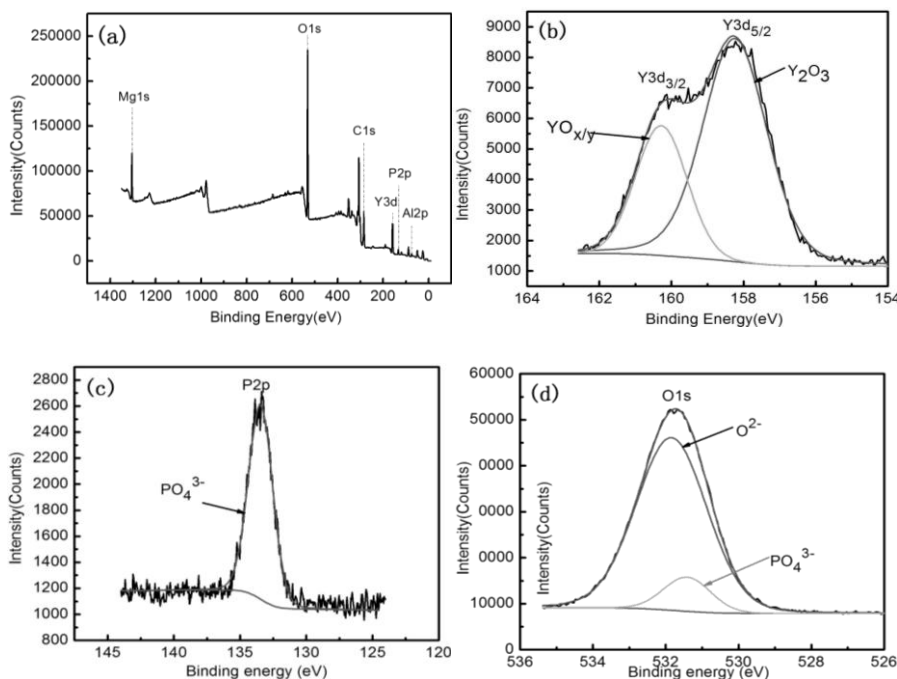


Figure 5. XPS analysis of yttrium-based coating phosphated in solution containing 1.5% mass fraction of $NH_4H_2PO_4$ at 80 °C for 120s (a) survey scanning spectrum, (b) high-resolution spectrum of Y 3d, (c) high-resolution spectrum of P 2p and (d) high-resolution spectrum of O 1s

The O 1s spectrum is depicted in Fig. 5(d). It is well known that peaks at about 530 eV are due to oxides and the peak at about 532 eV is attributed to oxygen species dissolved in the metal or to

adsorbed oxygen or OH⁻ group [29]. Therefore the O 1s lines positioned at 531.83 eV and 531.39 eV are the characteristics of oxide. Therefore, it can be concluded that the phosphated yttrium-based coatings are mainly composed of yttrium oxides and phosphate oxide, which are consistent with the results of XRD and EDS.

3.3 Corrosion resistance properties of the coatings

In order to evaluate the corrosion resistance properties of the coatings, the electrochemical measurements of uncoated AZ91D sample, the yttrium-based conversion coating and the phosphated coating in 3.5 wt.% NaCl solution at room temperature were conducted.

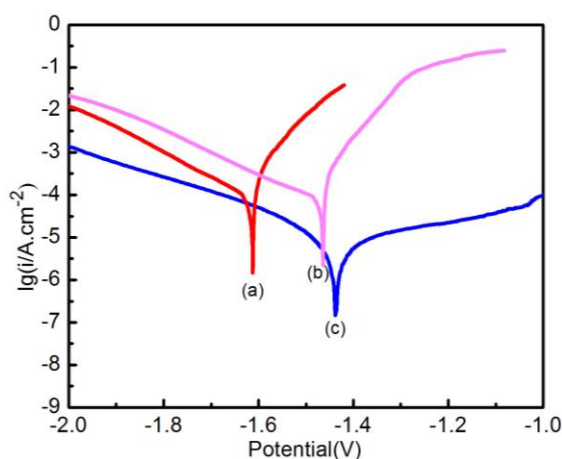


Figure 6. Potentiodynamic curves of AZ91D magnesium alloy (a) uncoated, (b) immersed in solution containing 10g/L Y(NO₃)₃ at 30 °C for 50min and (c) immersed in solution containing 10g/L Y(NO₃)₃ at 30 °C for 50min and then in solution coating 1.5% mass fraction of NH₄H₂PO₄ at 80 °C for 120s

It is well known that corrosion current density (I_{corr}) and corrosion potential (E_{corr}) are frequently used to evaluate corrosion resistance of the samples. For the polarization curves, the anodic curve is the important feature related to the corrosion resistance, while the cathodic reaction corresponds to the evolution of hydrogen [30, 31].

Table 3. Tafel fitting results of potentiodynamic curves shown in Figure 6

Material	E_{corr} (mV)	$I_{corr}/area(\mu A/cm^2)$	b_c (mV/dec)
Uncoated sample	-1610	70.2	256.1
Conversion coating	-1460	58.8	189.5
Phosphated conversion coating	-1430	7.7	162.3

It is found that the hydrogen evolution rate of the yttrium-based conversion coating decreases after phosphating.

The corrosion current density of uncoated alloy increases quickly with increasing potential, indicating that the active dissolution of magnesium substrate [32]. It can be found from the polarization curves in Fig. 6 that the phosphated sample slows down the corrosion rate of the conversion coating by inhibiting both the cathodic hydrogen evolution and anodic dissolution reactions. The Tafel fitting results of the uncoated sample, the conversion coating and the phosphate sample are listed in Table 3. It can be found that the I_{corr} of the phosphated sample is about $7.7\mu A \cdot cm^{-2}$, which is less about one order of magnitude than the uncoated alloy and the conversion coating. The E_{corr} of the phosphated sample is increased about 30 mV compared to the yttrium-based conversion coating and 180 mV compared to uncoated sample

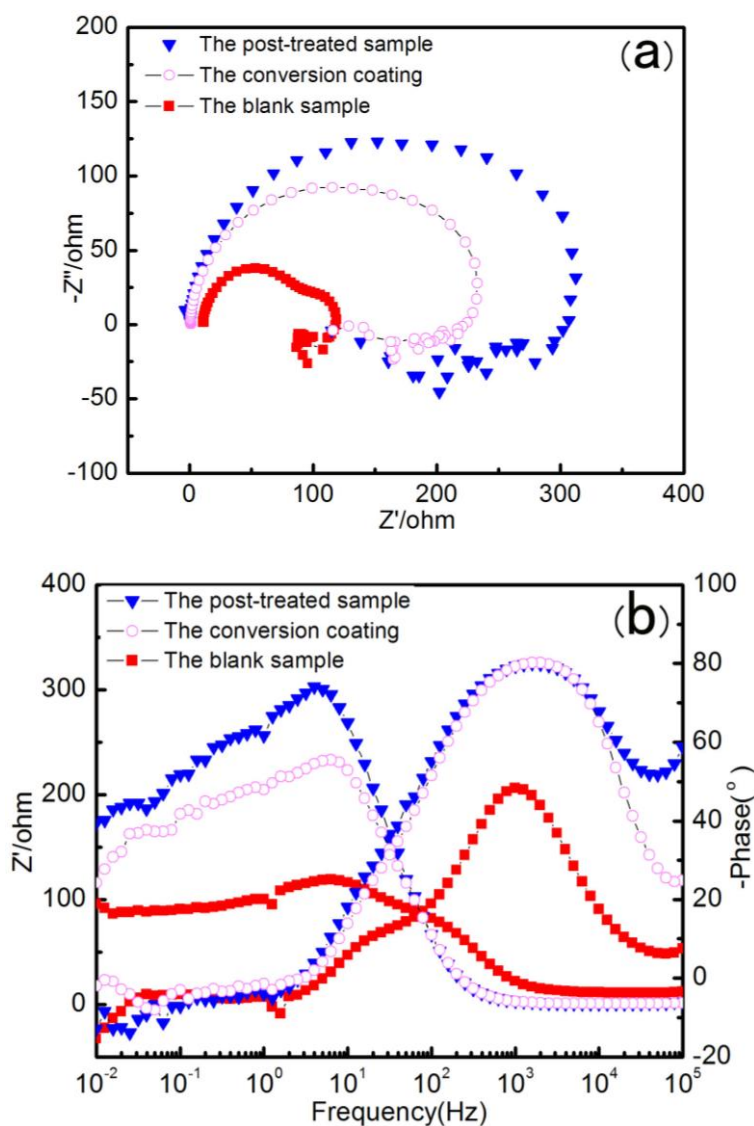


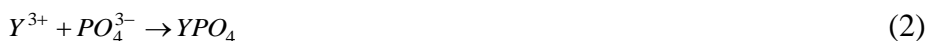
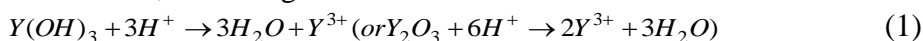
Figure 7. Nyquist plots (a) and Bode phase plots (b) obtained during immersion in 3.5 wt.% NaCl solution at room temperature of uncoated AZ91D magnesium alloy, yttrium-based coating and phosphated yttrium-based coating respectively

In order to evaluate the corrosion inhibition effect of the phosphated sample, electrochemical impedance spectroscopy (EIS) measurement which is a non-destructive technique was proposed as a tool to follow up the stationary behavior of metallic materials [33]. In present investigation, EIS was performed for AZ91D magnesium alloys after the stabilization of the open circuit potential (OCP) immersion in 3.5 wt% NaCl solution. In order to compare, the EIS measurements are performed on both uncoated AZ91D magnesium alloy substrate and yttrium-based conversion coating. The representative impedance spectra of the uncoated sample, the yttrium-based conversion coating and the phosphated sample are recorded in Fig. 7. The Nyquist plots (Fig. 7a) contain two capacitive loops at high and medium frequencies and one low frequency inductive loop. Therefore, it can be assumed that the overall response of the system is associated with loop. However, the loop from the double layer forms at metal solution interface and the loop due to the relaxation of adsorbed species appears on the substrate surface [34]. There is obvious difference in the size of the capacitive loop among these samples is. The diameter of capacitive loop is associated with the charge-transfer resistance and with the corrosion resistance [35]. The Bode phase angle plots (Fig. 7b) show three constants for uncoated sample, and two constants for both conversion coating and phosphated sample. Noticeably, the phosphated sample displays higher value. On the basis of above analysis, it can be inferred that the total impedance value of the phosphated sample is much higher. Therefore the phosphated sample possesses better corrosion resistance than uncoated sample and yttrium based conversion coating.

3.4 Phosphating mechanism

Immediately after soaking the yttrium-based conversion sample in the $\text{NH}_4\text{H}_2\text{PO}_4$ solution, yttrium-based coating will slightly dissolve, especially that in the cracks and flaws. Simultaneously, As reported in Reference [36-38] Mg of yttrium conversion coating in the crack will dissolve and the hydrogen will be released.

At the same time, the free phosphate ion can react with Mg ion in the solution to form magnesium orthophosphate which deposits on the cracks and flaws. This results in the reduction of the crack numbers and the improvement of the film performance. With the process of reaction, hydrogen ion diffuses to the film surface, and phosphate ion adsorbs on the surface of yttrium conversion coatings. Therefore, following reactions will occur:



According to the above reaction, part of the coating will dissolve and correspondingly some stable phosphate compound such as YPO_4 , AlPO_4 and $\text{Mg}_3(\text{PO}_4)_2$ will generate. Further, the size and the number of the cracks will decrease during the process of drying. As a result of repair effect of the $\text{NH}_4\text{H}_2\text{PO}_4$ on the yttrium-based conversion coating, the composite coating shows compactness and better corrosion resistance.

4. CONCLUSIONS

A composite conversion coating on the AZ91D Mg alloy was prepared by simply dipping the yttrium-based conversion coating into $\text{NH}_4\text{H}_2\text{PO}_4$ solution. The results are summarized as follows:

(1) The yttrium-based coating, which acts as a barrier to environment, improves the corrosion resistance of the AZ91D Mg alloy in some extent. Then the densification process is achieved by $\text{NH}_4\text{H}_2\text{PO}_4$ to further improve corrosion protection of AZ91D Mg alloy.

(2) The compactness of the yttrium conversion coatings after phosphating is improved, which benefits to reduce the number and size of the cracks. And the repair effect of the $\text{NH}_4\text{H}_2\text{PO}_4$ on the yttrium-based conversion coating shows better corrosion resistance.

(3) The phosphated composite coatings are mainly consisted of Y_2O_3 , YO_x/y , MgPO_4 , AlPO_4 and YPO_4 .

ACKNOWLEDGEMENT

This work was jointly supported by the Ground Plan of Science and Technology Projects of Jiangxi Province, China (Grant No. KJLD2013078) and Open Project of Jiangxi Provincial Engineering Research Center for Magnesium Alloys (2015).

References

1. Zhang B.P, Tu Y.F, Chen J.Y, Zhang H.L, Kang Y.L and Suzuki H.G, *J. Mater. Process. Technol.*, 184 (2007)102.
2. Su J, Sanjari M, Kabir A.S.H, I.-H. Jung, Jonas J.J, Yue S and Utsunomiya H, *Mater. Sci. and Eng. A*, 636 (2015) 582.
3. Gutman E.M, Eliezer A and Unigovski Abramov Y.E, *Mater. Sci. Eng. A*, 302 (2001) 63.
4. Song W.W, Martin H.J, Hicks A, Seely D, Walton C.A, Lawrimore II W.B, Wang PT and Horstemeyer M.F, *Corros.Sci.*, 78 (2014) 353.
5. Ramezanzadeh B , Vakili H and Amini R, *J. Ind. Eng. Chem.*, 30 (2015) 225.
6. Zhang D.F, Gou Y.N, Liu Y.P and Guo X, *Surf. Coat.Technol.*, 236 (2013) 52.
7. Kuo Y.L and Chang K.H, *Surf. Coat. Technol.*, 283 (2015) 194.
8. Hu J.Y, Li Q, Zhong X.K, Li L.Q and Zhang L, *Thin Solid Films*, 519 (2010) 1361.
9. Yan D.L, Yu G, Hu B.N, Zhang J, Song Z.W and Zhang X.Y, *J. Alloys Compd.*, 653 (2015) 271.
10. Harada Y and Kumai S, *Surf. Coat.Technol.*, 228 (2013) 59.
11. Xu N and Bao Y.F, *Mater. Sci. Eng. A*, 655 (2016) 292.
12. Cui X.F i, Jin G, Li Q.F, Yang Y.Y, Li Y and Wang F.H, *Mater. Chem. Phys.*, 121 (2010) 308.
13. Qingjiang M and Frankel G.S, *Surf. Interface Anal.*, 36 (2004) 30.
14. Lee Y.L, Chu Y.R, Li W.C and Lin C.S, *Corros.Sci.*, 70 (2013) 74.
15. Jian S.Y, Chu Y.R and Lin C.S, *Corros. Sci.*,93 (2015) 301.
16. Li K., Liu J.Y, Lei T and Xiao T, *Appl. Surf. Sci.*, 353 (2015) 811.
17. Hamdy A.S and Butt D.P, *Electrochim. Acta*, 108 (2013) 852.
18. Yang L.H, Li J.Q, Yu X, Zhang M.L and Huang X.M, *Appl. Surf. Sci.*, 255 (2008) 2338.
19. Wang X.M, Zhu L.Q, He X and Sun F.L, *Appl. Surf. Sci.*, 280 (2013) 467.
20. Zhang K, Ning SH, Ren C, Luo XW, Dong L X, Chen H and He YD, *Surf. Coat. Technol.*, 266 (2015) 105.
21. Ang C, Seeber A , Williams T and Cheng Y.B, *J. Eur. Ceram. Soc.*, 34 (2014) 2875.
22. H.F. Gao, H.Q. Tan, J. Li, Y.Q. Wang and J.Q. Xun, *Surf. Coat. Technol.*, 212 (2012) 32.
23. Chen L, Chen C.G, Wang N.N, Wang J.M and Deng L, *Rare Metal Mater. Eng.*, 44(2015) 0333.

24. Zhang M, Cai S, Shen S.B, Xu G.H, Li Y, Ling R.and Wu X.D, *J. Alloys Compd.*, 658 (2016) 649.
25. Liu J.R, Guo Y.N and Huang W.D, *Surf. Coat. Technol.*, 201 (2006) 1536.
26. Hayoz,J philo T, Bovet M., Züttel A, Guthrie S, Pastore G, Schlapbach L and Aebi P, *J. Vac. Sci. Technol. A*, 18 (2000) 2417.
27. Mohamed,S and Raaif H M, *Surf. Coat. Technol.*, 205 (2010) 525.
28. Ishizaki, Kudo T R, Omi, Teshima T K, Sonoda T, Shigematsu I and Sakamoto M, *Electrochim. Acta*, 62 (2012) 19.
29. Choi J.G and Thompson L.T, *Appl. Surf. Sci.*, 93 (1996) 143.
30. Gu C.D, Lian J.S, He J.G, Jiang Z.H and Q. Jiang, *Surf. Coat. Technol.*, 200 (2006) 5413.
31. Rajabalizadeh Z and Seifzadeh D, *Prot. Met. Phys. Chem.*, 50 (2014) 516.
32. Yang X.W, Wang G.X, Dong G.J, Gong F and Zhang M.L, *J. Alloys Compd.*, 487 (2009) 64.
33. Lei L, Shi J, Wang X, Liu D and Xu H.G, *Appl. Surf. Sci.*,376 (2016) 161.
34. Santamaria M., Quarto F. Di, Zanna S and Marcus P, *Electrochim. Acta*, 53(2007) 1314.
35. Chen,L. Chen C.G, Wang N.N, J.M. Wang and Deng L, *Rare. Metal. Mat. Eng.*, 44 (2015) 0333.
36. Li L.J, Lei J.L, Yu S.H, TianY.J, Jiang Q.Q, and Pan F.S, *J. Rare Earth*, 26 (2008) 383.
37. Jiang X, Guo R.G and Jiang S.Q, *Appl. Surf. Sci.*,341 (2015) 166.
38. Wang C, Zhu S.L, Jiang F, and Wang F.H, *Corros. Sci.*,51 (2009) 2916.

© 2016 The Authors. Published by ESG (www.electrochemsci.org). This article is an open access article distributed under the terms and conditions of the Creative Commons Attribution license (<http://creativecommons.org/licenses/by/4.0/>).